

Article

Measurement of ^{15}N relaxation in the detergent-solubilized tetrameric KcsA potassium channel

Jordan H. Chill, John M. Louis, James L. Baber & Ad Bax*

Laboratory of Chemical Physics, NIDDK, National Institutes of Health, Building 5, Room 126, 9000 Rockville Pike, Bethesda, Maryland 20892, USA

Received 2 June 2006; Accepted 26 July 2006

Key words: backbone dynamics, cross correlation, diffusion anisotropy, micelle, relaxation interference, rotational correlation time, selectivity filter

Abstract

A set of TROSY-HNCO (tHNCO)-based 3D experiments is presented for measuring ^{15}N relaxation parameters in large, membrane-associated proteins, characterized by slow tumbling times and significant spectral overlap. Measurement of backbone ^{15}N R_1 , $R_{1\rho}$, $^{15}\text{N}\{-^1\text{H}\}$ NOE, and ^{15}N CSA/dipolar cross correlation is demonstrated and applied to study the dynamic behavior of the homotetrameric KcsA potassium channel in SDS micelles under conditions where this channel is in the closed state. The micelle-encapsulated transmembrane domain, KcsATM, exhibits a high degree of order, tumbling as an oblate ellipsoid with a global rotational correlation time, $\tau_c = 38 \pm 2.5$ ns, at 50 °C and a diffusion anisotropy, $D_{\parallel}/D_{\perp} = 0.79 \pm 0.05$, corresponding to an aspect ratio $a/b \geq 1.4$. The N- and C-terminal intracellular segments of KcsA exhibit considerable internal dynamics (S^2 values in the 0.2–0.45 range), but are distinctly more ordered than what has been observed for unstructured random coils. Relaxation behavior in these domains confirms the position of the C-terminal helix, and indicates that in SDS micelles, this amphiphilic helix does not associate into a stable homotetrameric helical bundle. The relaxation data indicate the absence of elevated backbone dynamics on the ps–ns time scale for the 5-residue selectivity filter, which selects K^+ ions to enter the channel.

Introduction

It is becoming increasingly recognized that the mode of action of biological macromolecules is determined not only by their static three-dimensional structure, but to a significant extent also by dynamic perturbations from their equilibrium state (Wand, 2001; Kern and Zuiderweg, 2003). This realization has motivated the development of methods for the study of protein dynamics in terms of quantitatively measured, characteristic

parameters. NMR spectroscopy is capable of addressing protein dynamics on a wide range of timescales and in a site-specific manner. Multi-dimensional, indirect detection schemes have proven to be particularly valuable for probing such motions in proteins (Kay et al., 1989; Kay, 1998; Wagner and Nirmala, 1989; Ishima and Torchia, 2000; Palmer, 2001; Akke, 2002). Most commonly, protein backbone motions on the ps–ns timescale are followed using relaxation parameters of amide ^{15}N nuclei. Experimental protocols for measuring backbone ^{15}N relaxation (Farrow et al., 1994; Palmer et al., 2001; Kempf and Loria, 2003) as well as the theoretical framework for interpretation of

*To whom correspondence should be addressed. E-mail: bax@nih.gov

their results (Lipari and Szabo, 1982; Clore et al., 1990; Peng and Wagner, 1992; Farrow et al., 1995; Mandel et al., 1995; Renner et al., 2001; Bruschweiler, 2003) are well-known and two-dimensional NMR measurements are being used routinely for proteins up to 30 kDa in size. This versatile approach has been used to explore several aspects of protein dynamics, including exchange processes (Grey et al., 2003), low-population excited states (Mulder et al., 2001; Korzhnev et al., 2003), and enzyme kinetics (Eisenmesser et al., 2002).

In larger proteins, however, rapid decay of signal and increasing spectral overlap limits the effectiveness of such methods, motivating the use of 3D HNCQ-based (Caffrey et al., 1998) and accordion-based (Carr et al., 1998) methods. In this context, α -helical membrane-associated proteins represent an important case in point. Membrane proteins require the hydrophobic environment of the cellular membrane, or mimics thereof, to maintain their structural stability and functionality. As a result, study of dynamics in this class of proteins presents high-resolution NMR with unique difficulties. Studied in large macro-assemblies of detergent micelles, even proteins of intermediate size quickly challenge the sensitivity and resolution limitations of NMR (Arora and Tamm, 2001). This is particularly true for helical membrane proteins, which typically suffer from poor spectral dispersion. In addition, the presence of significant detergent concentrations in the NMR sample (typically on the order of ~ 100 mM) may complicate the acquisition of high quality NMR data. A recent, new approach has utilized ^2H relaxation measurements in specifically labeled methyl groups to investigate side-chain dynamics in an 82-kDa enzyme (Tugarinov et al., 2005). This approach is expected to also be applicable to large helical membrane proteins such as KcsA, in particular in view of the fact that assignments for many methyl groups in this system have been reported recently (Yu et al., 2005). However, the utility of NMR in studying backbone dynamics in large membrane proteins depends on the development of methods tailored to the requirements of these systems.

Here we present modifications of the HNCQ-based experiments (Caffrey et al., 1998) designed and optimized for measurement of the standard ^{15}N relaxation parameters (R_1 , $R_{1\rho}$, and NOE) in large membrane proteins. Rapid estimations of the

relaxation rates are achieved by measuring only two points for appropriate values of the relaxation periods. The TROSY-HNCQ (tHNCQ) block used for read-out of the various signals is tailored for NMR samples containing protonated detergent, when using a cryogenic probe. A variant of this experiment is proposed for convenient and rapid measurement of the cross-correlation between ^{15}N chemical shift anisotropy (CSA) and ^{15}N - ^1H dipolar relaxation mechanisms. Technical aspects and advantages of these relaxation experiments are discussed. The practical application of these methods is demonstrated on the homotetrameric KcsA potassium channel under conditions where the channel is believed to be in the closed state (Cuello et al., 1998; Heginbotham et al., 1999). The tetramer is solubilized in SDS micelles, resulting in mixed micelles estimated to have a total mass of *ca.* 120 kDa (Chill et al., 2006). The proposed experiments enable us to obtain site-specific relaxation measurements despite the severely overlapping nature of the ^1H - ^{15}N -correlation spectrum of KcsA. The results are evaluated in the context of the known structure of KcsA (Doyle et al., 1998) with particular emphasis on the extra-micellar C-terminal region, for which no detailed structural characterization is yet available, and the pore-entrance segment, which is critical to channel selectivity for K^+ ions.

Methods

NMR samples

The KcsA potassium channel was expressed and purified as previously described (Chill et al., 2006). Since back-exchange of protons into amide sites embedded within the SDS micelle could not be achieved, two complementary samples were prepared. In the first case, a sample of uniformly labeled ^2H , ^{13}C , ^{15}N -KcsA in H_2O contained protonated exchangeable amide sites, whereas amide sites within the micelle remained deuterated. In the second case, KcsA was expressed in H_2O under conditions which minimized the biosynthetic incorporation of protons at aliphatic sites (Lohr et al., 2003). Subsequently transferred to D_2O , this sample contains protonated amide sites within the micelle only, while exchangeable sites were deuterated (McCallum et al., 1999). These

samples are designated KcsA^E and KcsATM, respectively. Typical samples contained 0.2–0.3 mM KcsA (tetramer concentration) solubilized in SDS ([SDS]:[KcsA₄] maintained at 600–800:1) in 25 mM MES at pH 6.0. For NMR measurements 300–350 μ l of sample were placed in a thin-wall Shigemi microcell (Shigemi Inc., Allison Park, PA).

Pulse sequences

In designing experiments for measurement of backbone ¹⁵N relaxation parameters suitable for larger membrane proteins, three important considerations were addressed: (i) With sensitivity and resolution at a premium, it is imperative that signal readout employs the TROSY principle (Pervushin et al., 1998); (ii) Large proteins, particularly helical membrane proteins, require a ¹³C'-modulated signal readout (3D HNCO) to minimize loss of residue-specific information caused by resonance overlap (Caffrey et al., 1998); (iii) The increasingly routine use of cryogenic probes in the study of large proteins requires precise handling of water magnetization, favoring sequences that include coherence selection gradients, and that keep water aligned along the +z axis. The presence of a large excess of detergent accentuates the importance of gradient selection, since its deuteration may not be cost-effective. In addition, spin diffusion between detergent protons, an important reservoir of rapidly relaxing ¹H magnetization, and amide protons in the membrane protein increases the rate at which the experiments can be repeated.

Measurement of R_1 , $R_{1\rho}$ and $^{15}\text{N}-\{^1\text{H}\}$ -NOE

Figure 1 shows the sequences designed to measure R_1 , $R_{1\rho}$, and the steady-state $^{15}\text{N}-\{^1\text{H}\}$ -NOE (hetNOE) for backbone ¹⁵N nuclei. The three sequences are based on well-known relaxation experiments (Kay et al., 1989; Farrow et al., 1994; Zhu et al., 2000), but use the tHNCO experiment for signal readout, thereby spreading the ¹H–¹⁵N correlation map along a third dimension. Briefly, in the R_1 and $R_{1\rho}$ experiments (panels A–B) the appropriate in-phase ¹⁵N operator is prepared by point *a*, and decay occurs for a given variable time Δ . By point *b* an anti-phase ¹³C' operator (with respect to ¹⁵N) has been created, leading back into an HNCO-type experiment with constant time ¹⁵N

evolution. The TROSY element beginning at point *c* combines the advantages of multiple water flip-back pulses (Pervushin et al., 1998) and gradient coherence selection (Pervushin et al., 1998; Weigelt, 1998; Tian et al., 2005) into a single streamlined experiment which gives excellent suppression of water and detergent signal. Note that only the slowly relaxing ¹⁵N component is selected from this point onwards; during the relaxation delay the in-phase ¹⁵N operator is unaffected by ¹H spin-flips for longitudinal relaxation, and decays at the average rate of its two components for transverse relaxation. The TROSY element normally uses either a two-step phase cycle or coherence-selecting gradients to obtain the echo-anti-echo spectrum (Pervushin et al., 1998). In our implementation, we use very weak coherence-selecting gradients, in combination with the two-step phase cycle, which in our experience yields improved results on cryogenic probeheads.

In the case of the steady-state $^{15}\text{N}-\{^1\text{H}\}$ -NOE experiment (panel C), amide protons are saturated (NOE experiment) or left untouched (NONOE experiment) in alternately acquired FIDs. Steady-state ¹⁵N magnetization is then converted into anti-phase ¹³C' magnetization at the start of the t_1 evolution period, and is followed by the tHNCO readout scheme. The need for a ¹H 90° pulse prior to the first ¹⁵N 90° pulse in the NONOE branch has been previously noted (Zhu et al., 2000). Briefly, in slowly tumbling proteins such as the KcsA tetramer, ¹⁵N T_1 relaxation times are very long (ca 3s for the KcsATM domain), and relaxation of the downfield TROSY (even longer T_1) and upfield anti-TROSY (shorter T_1) components differ significantly. Without mixing these two components immediately prior to ¹⁵N evolution or allowing both to fully relax, the reference signal (without NOE) would be too weak, leading to an erroneous NOE ratio. The 90° pulse, applied just before ¹⁵N evolution, to a good approximation removes this effect by mixing the two doublet components, without introducing sufficient time for $^{15}\text{N}-\{^1\text{H}\}$ NOE to build up.

Measurement of cross-correlated relaxation η_{xy}

It is well known that the interference between contributions of the ¹⁵N–¹H dipole–dipole (DD) interaction and ¹⁵N CSA to relaxation results in significantly different relaxation rates for the upfield

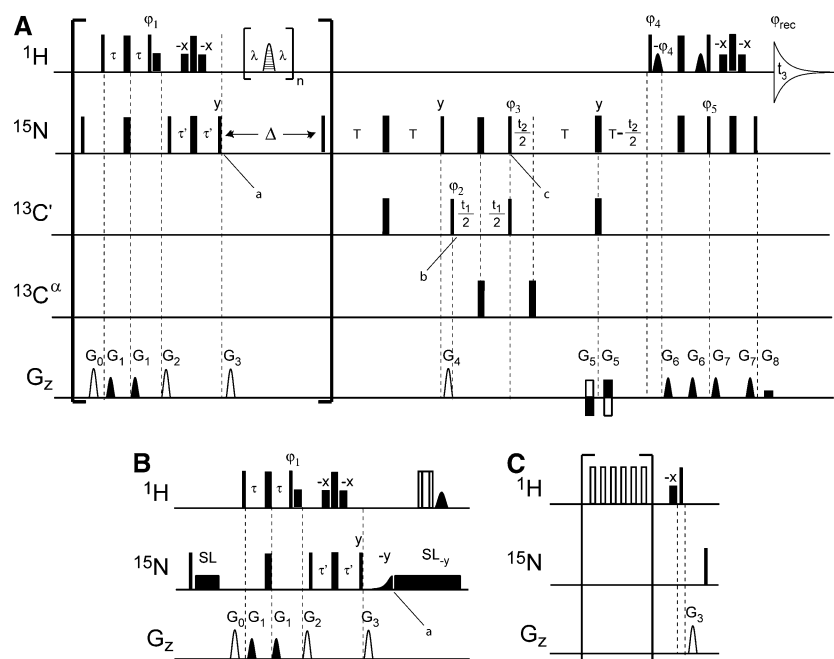


Figure 1. TROSY-HNCO-based pulse sequences for measuring ^{15}N relaxation parameters. Narrow (wide) pulses correspond to 90° (180°) flip angles with phase x , unless otherwise indicated. Water saturation is minimized by maintaining water magnetization along the $+z$ axis using selective 1 ms rectangular pulses (low rectangles) and 1.6 ms shaped (center lobe of $\sin x/x$) pulses, applied on resonance with the solvent. The pulse width of all ^{13}C 90° (180°) pulses is adjusted to $\sqrt{15/[4*\omega]}$ ($\sqrt{3}/[2*\omega]$), where ω is the frequency difference in Hz between the centers of the $^{13}\text{C}'$ and $^{13}\text{C}^\alpha$ regions. Delay durations: $\tau = \tau' = 2.4$ ms; $T = 12.5$ ms. Pulsed magnetic field gradients with sine-bell profiles applied along the z -axis include open bell-shaped gradients, which select the $N_z H_z$ longitudinal two spin order, and pairs of filled bell-shaped gradients, which select single-quantum type coherences throughout the sequence. The rectangular gradients G_5 and G_8 select the desired coherence in the TROSY block and effectively filter out spurious detergent signals. Gradient amplitudes and durations: (G/cm, ms) are: G_0 , 12, 2.5; G_1 , 9, 0.4; G_2 , 12, 1.5; G_3 , 13.8, 2; G_4 , 10.8, 2; G_5 , -18, 0.2; G_6 , -9, 0.4; G_7 , 18, 0.4; G_8 , 18, 0.04. (A) Sequence for measuring ^{15}N longitudinal relaxation R_1 . The hatched bell-shaped pulse is a 1.8 ms-long IBURP pulse applied on resonance with the $^1\text{H}^N$ protons. The delay λ is set to 3.1 ms and the sequence (λ -IBURP- λ) is repeated n -fold, so that longitudinal relaxation occurs for a time $\Delta = n \times 8$ ms. Phase cycling is as follows: $\phi_1 = 2(y)$, $2(-y)$; $\phi_2 = x$, $-x$; $\phi_3 = y$; $\phi_4 = \phi_5 = y$; $\phi_{\text{rec}} = y$, $-y$, $-y$, y ; G_5 and G_8 have opposite polarity. For quadrature in the ^{15}N dimension a second FID is acquired for each t_2 delay, with $\phi_4 = \phi_5 = -y$ and where G_5 and G_8 have the same polarity, and the data are processed in echo/anti-echo fashion. Quadrature in the $^{13}\text{C}'$ dimension is obtained by States-TPPI incrementation of ϕ_2 . In the interest of maintaining a four-step phase cycle, the optional TROSY two-step cycle (Pervushin et al., 1998) was omitted from the R_1 experiment to allow for a two-step cycling of the second ^1H 90° pulse, which is necessary to eliminate contributions of ^{15}N steady-state magnetization (B) Preparation block for measurement of ^{15}N transverse relaxation in the rotating frame $R_{1\rho}$. ^{15}N spins are adiabatically flipped to the transverse plane using a 1.8 ms half-hyperbolic secant pulse (1.8 kHz peak power), and then locked using a 1.8 kHz RF field. Possible RF-heating effects arising from the spin-lock pulse are corrected by preceding the ^1H excitation with a ^{15}N pulse of identical power, and a duration which maintains the overall spin-locking time constant in the reference and attenuated experiments. Inversion of $^1\text{H}^N$ during the spin-locked relaxation utilizes a composite ($90x - 180y - 90x$) pulse, followed by a 180-degree flip back of the solvent, and serves to eliminate contributions from cross-correlated relaxation. For longer spin-lock durations (on the order of the reciprocal of the proton spin-flip rate) multiple $^1\text{H}^N$ inversions should be employed. Quadrature detection is obtained similarly to (A). Phase cycling is as follows: $\phi_1 = y$; $\phi_2 = x$, $-x$; $\phi_3 = y$, x ; $\phi_4 = \phi_5 = y$; $\phi_{\text{rec}} = y$, $-x$, $-y$, x ; G_5 and G_8 opposite polarity. In alternating acquisitions, $\phi_3 = y$, $-x$; $\phi_4 = \phi_5 = -y$; G_5 and G_8 same polarity. (C) Preparation block for measurement of the steady-state ^{15}N - ^1H NOE. $^1\text{H}^N$ saturation in the NOE part of the experiment is effected by repetition of a ^1H 150° flip angle pulse followed by a 15 ms delay. An equivalent delay replaces the saturation period in the NONOE part of the experiment. Phase cycling and quadrature detection are identical to (B). In cases where ^{15}N spectral resolution is not limiting, an additional gain in sensitivity can be obtained by using the first half of the TROSY element for rephasing of $^{13}\text{C}'$ - ^{15}N coupling, permitting a correspondingly shorter duration of the ^{15}N constant time evolution period (Loria et al., 1999).

and downfield components of the ^{15}N signal (Goldman, 1984). The transverse cross-correlated relaxation term η_{xy} , defined as half the difference between these two rates, can be readily interpreted in terms of protein motions. This is because other

effects such as interactions with distant protons and exchange contributions affect both individual rates equally and therefore are conveniently eliminated from their difference (Kroenke et al., 1998; Tjandra et al., 1996; Lee et al., 2006). Figure 2 shows a

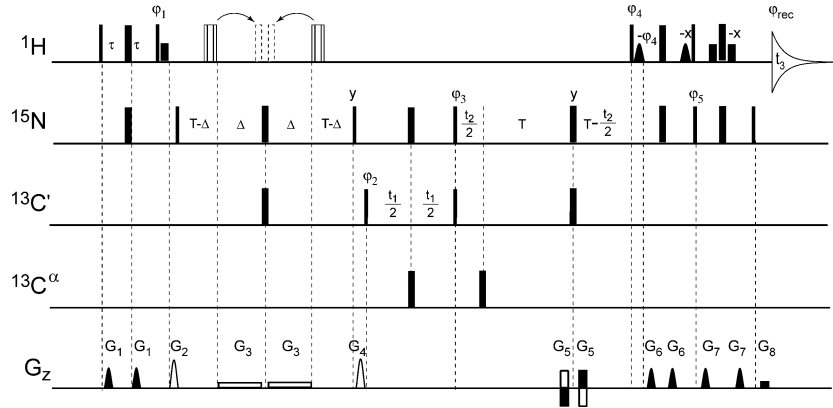


Figure 2. TROSY-HNCO-based pulse sequence for measuring ^{15}N cross-correlation. All pulses, gradients, and delays follow the definitions of Figure 1. Open rectangles represent composite $90^\circ x - 180^\circ y - 90^\circ x$ ^1H pulses, which invert amide protons during the first ^{15}N - $^{13}\text{C}'$ dephasing period. Two spectra are recorded in interleaved fashion. Whereas in the reference spectrum the two composite ^1H pulses are applied immediately adjacent to the ^{15}N 180° pulse, in the attenuated spectrum they are shifted by a delay Δ on either side of the ^{15}N pulse, with Δ being an integral multiple of $(2J_{\text{NH}})^{-1}$. A weak gradient ($G_3 = 1\text{--}1.5$ G/cm) is applied throughout each of these delays to suppress radiation damping. Phase cycling is as follows: $\phi_1 = y$; $\phi_2 = x, -x$; $\phi_3 = y, x$; $\phi_4 = \phi_5 = y$; $\phi_{\text{rec}} = y, -x, -y, x$; G_5 and G_8 opposite polarity. For quadrature in the ^{15}N dimension a second FID is acquired for each t_2 delay, with $\phi_3 = y, -x$; $\phi_4 = \phi_5 = -y$, and where G_5 and G_8 have the same polarity, and the data are processed in echo/anti-echo fashion. Quadrature in the $^{13}\text{C}'$ dimension is obtained by States-TPPI incrementation of ϕ_2 .

modified tHNCO sequence, of the same type as those shown in Figure 1, designed to measure η_{xy} for large proteins while minimizing relaxation losses. The key to this measurement is the first $\text{N} \rightarrow \text{C}'$ dephasing time, T , typically set to 25 ms, during which the $\text{N}^+ \text{H}^\beta$ and $\text{N}^+ \text{H}^\alpha$ operators, decaying at rates $R_2^{(\beta)}$ and $R_2^{(\alpha)}$, respectively, may be interchanged by inverting the amide ^1H spins. We record two interleaved spectra, the first with minimal time between the two ^1H inversion pulses and the second in which they are separated by a delay 2Δ equaling an integral multiple of $(J_{\text{NH}})^{-1}$. Under such conditions second-order effects may be safely neglected (Ghose et al., 1999), and the ratio between the intensities of the two HNCO peaks, I_{att} and I_{ref} , is represented by

$$\frac{I_{\text{att}}}{I_{\text{ref}}} = \frac{\exp(-R_2^\beta(2\Delta)) \exp(-R_2^\alpha(T - 2\Delta))}{\exp(-R_2^\beta T)} \quad (1a)$$

which can be arranged to yield

$$\frac{I_{\text{att}}}{I_{\text{ref}}} = \frac{\exp(-R_2^\alpha(2\Delta))}{\exp(-R_2^\beta(2\Delta))} = \exp(-4\eta_{xy}\Delta) \quad (1b)$$

thereby directly yielding the interference term. In this fashion η_{xy} is measured in a site-specific

manner and in a three-dimensional spectrum, without requiring a dedicated preparation time which would result in additional relaxation losses. For large proteins with global correlation times $\tau_c > 25$ ns at 600 MHz, the zero-frequency spectral density term $J(0) = 0.4\tau_c$ is the dominant (99%) contribution to cross-correlated relaxation. Therefore, under the rigid body approximation, η_{xy} is a direct measure of τ_c , using the relation (Tjandra et al., 1996)

$$\eta_{xy} = \rho\sigma 4J(0)(3\cos^2\theta - 1)/2 \approx 1.4^* \rho\sigma\tau_c \quad (2)$$

with $\rho = (\mu_0/4\pi)\gamma_{\text{H}}\gamma_{\text{N}}h/(4\pi r_{\text{NH}}^3)$, $\sigma = \gamma_{\text{N}}B_0\delta_{\text{N}}/3$, γ_{H} and γ_{N} the gyromagnetic ratios of ^1H and ^{15}N , respectively, h representing Planck's constant, r_{NH} the ^1H - ^{15}N internuclear distance, B_0 the external field and δ_{N} the ^{15}N CSA, and assuming an angle $\theta = 16^\circ$ (Cornilescu and Bax, 2000) between the ^{15}N - ^1H bond and the CSA tensor in α -helices.

NMR measurements

All NMR measurements were conducted at 323 K on a DRX600 Bruker spectrometer ($\gamma_{\text{N}}B_0 = 60.8$ MHz) using a cryogenic triple-resonance probehead equipped with z-axis pulsed field gradients. The tHNCO-based relaxation experiments (Figures 1 and 2) were applied to the KcsA^E sample for obtaining the ^{15}N relaxation rates. Due to

the limited number of resonances and the more favorable spectral dispersion of KcsATM, its relaxation rates were measured using two-dimensional versions of the presented sequences with TROSY readout (*vide infra*). For each KcsA domain, a single reference experiment, recorded with the minimal setting for the relaxation delay, with adequate ($\geq \sim 100:1$ for KcsA^E; $\geq \sim 60:1$ for KcsATM) signal-to-noise required 20–30 hours. In the interest of maintaining reasonable total measurement times, we therefore opted to estimate relaxation parameters using a two-point calculation (Jones et al., 1996) rather than a multi-point fit. Since for $R_{1\rho}$ measurements the intensity of the reference spectrum can be highly sensitive to offset effects if the magnetization is not 100% parallel to the spin lock field, an adiabatic hyperbolic secant pulse was used to bring the magnetization parallel to the spin-lock field at the start of the relaxation decay (Mulder et al., 1998). Such a pulse is conveniently generated as the first half of a hyperbolic secant inversion pulse (Silver et al., 1984) available in the standard Bruker library. To optimize the accuracy of such two-point measurements, the delay Δ in the attenuated experiment was usually chosen as $\Delta \sim 1/R_{\text{est}}$, with R_{est} the estimated relaxation rate based upon a short 1D experiment (Jones et al., 1996). Detailed acquisition parameters appear in the Supplementary Material (Table S1).

Data analysis

Spectra were processed and analyzed using the NMRPipe/NMRDraw software suite containing appropriate peak-picking and spectral-analysis routines (Delaglio et al., 1995). Relaxation parameters were extracted from the ratios in tHNCO peak intensities in the reference and attenuated spectra, where the peak position in the attenuated spectrum was constrained to be identical to that in the reference spectrum (Viles et al., 2001). R_2 values were obtained from corrected $R_{1\rho}$ measurements using the relation $R_{1\rho} = R_2 \cos^2 \theta + R_1 \sin^2 \theta$, with $\tan \theta = (\Delta\omega/\gamma B_1)$, $\Delta\omega$ being the offset of a given ¹⁵N resonance and B_1 the strength of the spin-lock field. Relaxation parameters were analyzed using FastModelFree (Cole and Loria, 2003), and spectral density mapping followed commonly used procedures (Buevich et al., 2001).

Results and discussion

Backbone ¹⁵N relaxation rates of KcsA

Measurement of KcsA relaxation parameters was facilitated by a two-domain approach, based on the previously reported extreme differences in solvent exchange rates (larger than 8 orders of magnitude) between amide protons outside and inside the SDS micelle (Chill et al., 2006). The latter include the two transmembrane-spanning segments TM1 (residues 35–50) and TM2 (residues 88–107), and the pore-helix and selectivity filter (residues 65–79) (Doyle et al., 1998). Spectra acquired for samples of KcsATM in 99% D₂O exhibited only peaks originating from amide sites in this micelle-encompassed domain, and were considerably simplified by the absence of signals from the exposed KcsA^E domain. For maximizing signal-to-noise it was beneficial to measure KcsATM relaxation parameters R_1 , R_2 and hetNOE (Zhu et al., 2000, with minor modifications) and η_{xy} (see Supplementary material, Figure S1) using the more sensitive 2D TROSY-HSQC-based versions of these experiments. Relatively long measurement times (16–24 h) were still needed for sufficient signal-to-noise in the KcsATM two-dimensional spectra. Due to higher sensitivity of the tHNCO-based scheme for measurement of cross-correlated relaxation (Figure 2), KcsATM η_{xy} values could be measured using both 2D- and 3D-experiments, yielding similar results.

¹⁵N relaxation parameters measured for KcsA – R_1 , R_2 , hetNOE, and η_{xy} – are shown in Figure 3. By virtue of the 3D-tHNCO readout utilized in this study, the full four-parameter set could be measured for over 70% of non-proline backbone amide sites, while only $\sim 8\%$ were lost to spectral overlap (see Supplementary Material, Figure S2). Most incomplete sets correspond to amide sites close to the intracellular micelle interface and the two extracellular loops. Amide sites in these regions are detectable only in the KcsA^E sample, yet resemble KcsATM amide sites in their relaxation behavior. As a result, they suffer from lower signal-to-noise under measurement conditions optimized for the majority of KcsA^E amide sites. Typical uncertainties in KcsA relaxation rates were 4–8% in R_1 , R_2 and η_{xy} , and 6–8% for the hetNOE experiment, which starts from steady-state ¹⁵N magnetization and therefore suffers from

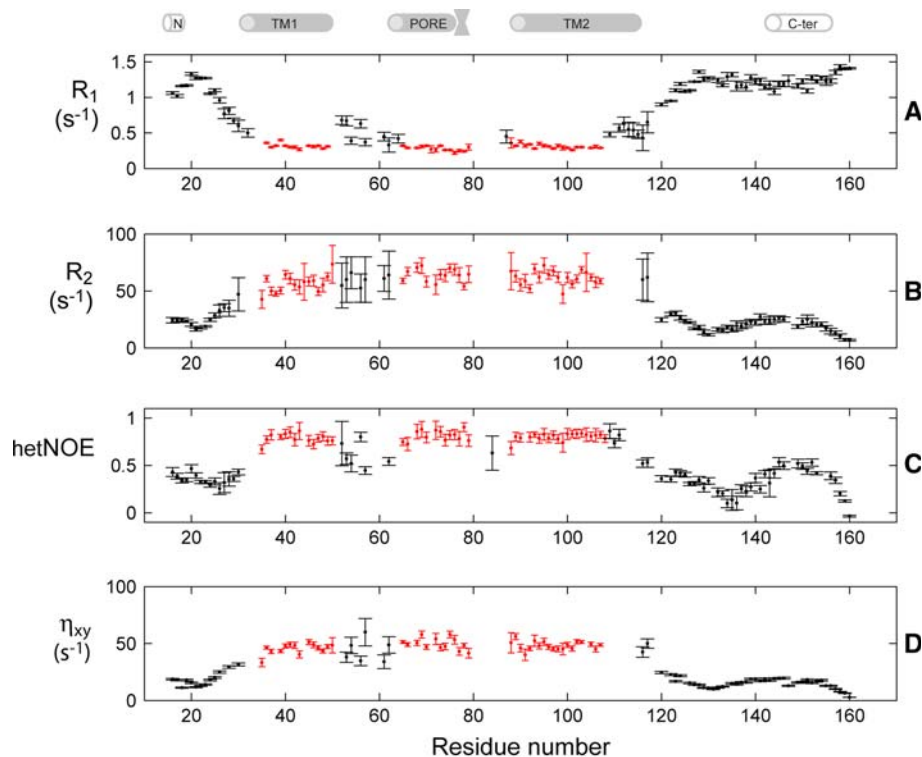


Figure 3. ^{15}N relaxation measurements for KcsA. (A) R_1 rates, (B) R_2 rates, (C) steady-state $^{15}\text{N}\{-^1\text{H}\}$ -NOE, and (D) cross-correlated relaxation η_{xy} rates measured for backbone ^{15}N nuclei of KcsA. All measurements were performed at a proton frequency of 600.13 MHz. Black and red error bars represent data acquired for the KcsA^E and KcsATM samples, respectively, prior to correcting for viscosity differences. Errors were estimated from noise levels in the spectra. Structural elements of KcsA (Doyle et al., 1998) appear above the data; helices are represented by rods and the selectivity filter is designated by the hourglass.

inherently lower sensitivity (see Supplementary Material, Table S2).

As highlighted in Figure 3, KcsA^E and KcsATM measurements were conducted in 7 and 99% D₂O, respectively, and therefore relaxation rates were obtained at different solvent viscosities. For purposes of analysis it is convenient to merge these measurements into a single dataset with uniform global relaxation behavior. This was accomplished by comparing relaxation rates across the boundaries between the two domains. Using $(R_2/R_1)^{1/2}$ as an estimate of τ_c at these amide sites, the solvent viscosity of the KcsATM sample was established as $23 \pm 7\%$ higher than that of its KcsA^E counterpart. The expected difference in solvent viscosity is 18% (Hardy and Cottington, 1949). Accordingly, KcsATM relaxation rates were adjusted to their corresponding values in 7% D₂O. Assuming slow-tumbling behavior, R_1 values were increased by 23% and R_2 and η_{xy} were decreased by a corresponding factor.

Anisotropic rotational diffusion of tetrameric KcsA

The membrane-spanning domain of KcsA can be represented as a prolate axially symmetric top, with its long axis coinciding with the four-fold symmetry axis, and characterized by principal inertia moments of 1.00:1.00:0.75 (Doyle et al., 1998). However, rotational diffusion of KcsA is also influenced by the micelle, which contributes 40–45% of the total molecular mass of the protein-micelle assembly (Chill et al., 2006). It is well established that anisotropy of rotational diffusion impacts ^{15}N relaxation rates, and therefore must be characterized in order to accurately translate these rates into backbone motions (Woessner, 1962; Schurr et al., 1994). KcsATM data are well-suited for this purpose, since its amide sites are typically quite rigid (hetNOE > 0.75), generally unaffected by exchange processes, and sample a sufficient angular range around the KcsA tetramer symmetry axis. Furthermore, it is reasonable to

assume that the diffusion of KcsATM is not highly anisotropic and that $\omega_N\tau_c \gg 1$, with $\tau_c = [6 \text{Tr}(D)]^{-1}$, thereby considerably simplifying the determination of the diffusion tensor (Lee et al., 1997; Copie et al., 1998). The correlation between the available R_1/R_2 ratios and orientations of KcsATM ^{15}N - ^1H bond vectors is shown in Figure 4. The observed pattern is consistent with the rotational diffusion of an oblate ellipsoid, with an overall global tumbling time of 47 ± 2 ns (in 99% D_2O) and D_{\parallel}/D_{\perp} ratio of 0.79 ± 0.06 , slightly below the theoretical minimal ratio of 0.796 (Cantor and Schimmel, 1980). Highly similar values (τ_c of 47.5 ns and D_{\parallel}/D_{\perp} of 0.80) were obtained when using model-free diffusion tensor optimization. We attribute the observed shift from a prolate shape of the tetramer to oblate rotational diffusion behavior to the effects of the SDS micelle upon KcsA diffusion. Although diffusion anisotropy is rather insensitive to the aspect ratio (a/b , where a and b are the long and short axes) in oblate ellipsoids, our data places a lower limit of $a/b > 1.4$ in SDS micelles containing the KcsA transmembrane domain (Cantor and Schimmel, 1980). We therefore conclude that the dominant contribution to relaxation is made by the KcsA-SDS assembly reorienting as an oblate rigid-body disc, whereas the contribution to relaxation of KcsA rotating as a prolate top within the micelle is negligible.

KcsA backbone motions on the ps–ns scale

^{15}N relaxation rates are commonly used to study backbone motions on the ps–ns scale. To this end, KcsA relaxation data were analyzed using spectral density mapping (Peng and Wagner, 1992; Farrow et al., 1995; Buevich et al., 2001) and the model-free (Lipari and Szabo, 1982; Mandel et al., 1995; Cole and Loria, 2003) approaches. Only residues for which coordinates were available in the X-ray structure were treated using the above derived anisotropic diffusion tensor. For residues without available coordinates, isotropic diffusion with $\tau_c = [6 \text{Tr}(D)]^{-1}$ was assumed. Results of these analyses are summarized in Figure 5 and Table S3 of the Supplementary Material. Both spectral density mapping and model-free analyses portray a continuous pattern of ps–ns motions along the KcsA backbone, despite the fact that data were acquired for two separate samples. The global tumbling correlation time τ_c predicted by relaxation data is 38 ± 2.5 ns (in 7% D_2O). This value is consistent with measurements of cross-correlated relaxation of amide protons in the KcsATM domain, for which typical values of $\eta_{xy} = 50 \pm 2 \text{ s}^{-1}$ were measured. Considering that the ^{15}N - ^1H bond and CSA tensor are nearly collinear, and that isotropic internal motions therefore may be described by a single internal correlation time (Tjandra et al., 1996), together with $S^2 = 0.92$ (Table 1), a global tumbling time of *ca.* 49 ns is

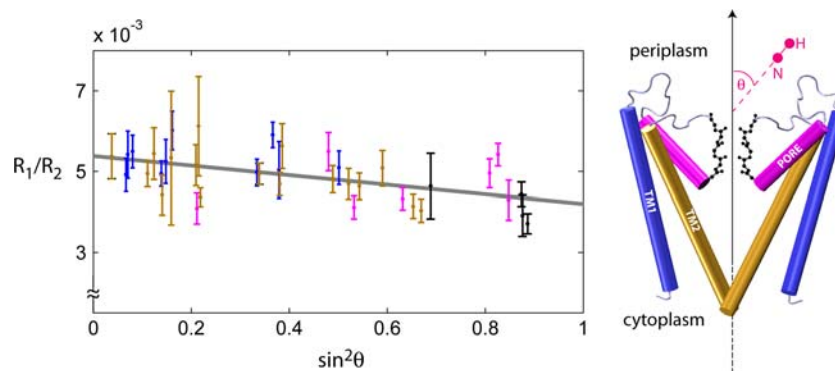


Figure 4. Rotational diffusion anisotropy of KcsA. ^{15}N R_1/R_2 ratios of all 38 well-resolved amide sites in the rigid KcsATM domain, excluding residue V76 shown to undergo exchange kinetics, are plotted against $\sin^2\theta$, where θ is the angle formed between the H–N bond-vector and the four-fold KcsA symmetry axis (PDB entry 1K4C). Residues in the TM1, pore, and TM2 helices are colored blue, magenta, and gold, respectively, and residues in the channel selectivity filter are in black (see illustration on right). Measurements were fitted to the line $1000*(R_1/R_2) = (5.38 \pm 0.19) - (1.16 \pm 0.30) * \sin^2\theta$, yielding $D_{\parallel} = (3.0 \pm 0.2) \times 10^6 \text{ s}^{-1}$, $D_{\perp} = (3.8 \pm 0.05) \times 10^6 \text{ s}^{-1}$, $\tau_c = (2D_{\parallel} + 4D_{\perp})^{-1} = 47 \pm 2$ ns and $D_{\parallel}/D_{\perp} = 0.79 \pm 0.06$. Uncertainties were determined by Monte-Carlo simulations and cross-validation methods with identical results.

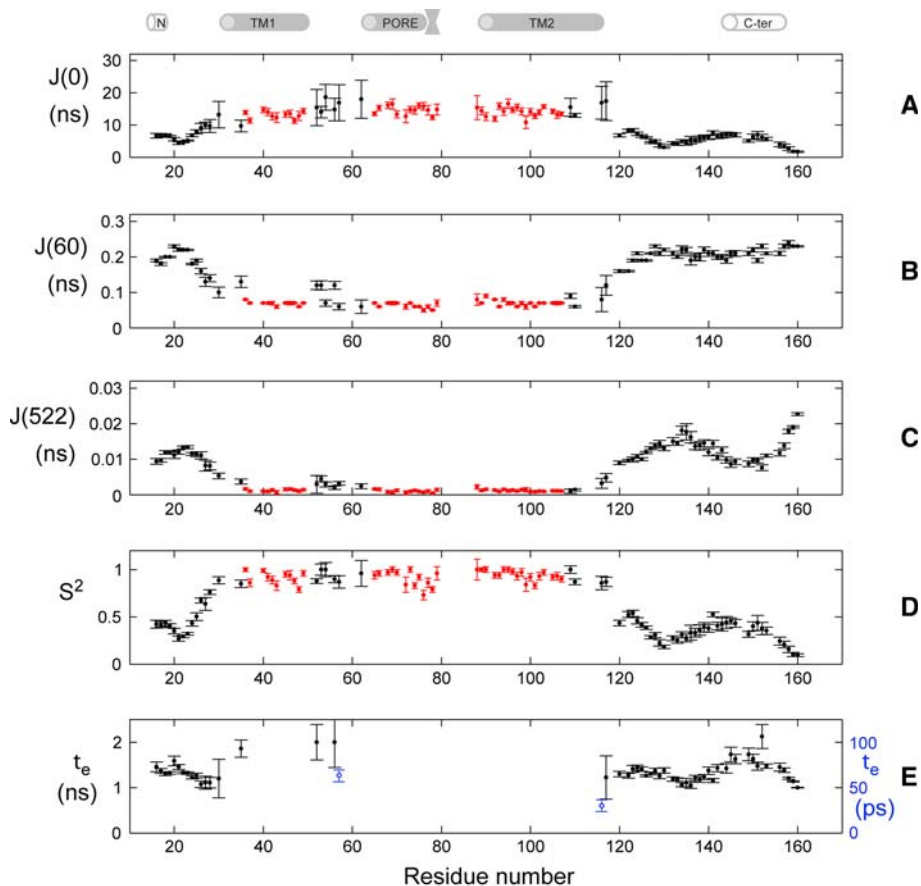


Figure 5. Analysis of ^{15}N relaxation data and ps–ns scale motions along the KcsA backbone. Summarized are the results of spectral density mapping (panels A–C) and the model-free approach (panels D–E) for KcsA. Values of (A) $J(0)$, (B) $J(\omega_{\text{N}})$, and (C) $J(0.87\omega_{\text{H}})$ are shown and calculated using standard formulae (Farrow et al., 1995). (D) Generalized squared order parameter S^2 , and (E) timescale of fast internal motions, τ_e , black and blue error bars representing ns and ps motions, respectively. For residues lacking structural coordinates (16–22, 125–160), model-free analysis used the global tumbling time of 38 ns and assumed isotropic rotational diffusion. Model-free analysis determines residue V76 to have an exchange contribution to R_2 . Structural elements of KcsA (Doyle et al., 1998) appear above the data; helices are represented by cylinders and the selectivity filter is designated by the hourglass.

obtained (in 99% D_2O), very similar to the value of 47 ± 2 ns obtained from the analysis of R_1/R_2 ratios. This good agreement demonstrates the utility of measuring η_{xy} during the initial characterization of a new system (Lee et al., 2006).

Described in general terms, four distinct regions along the KcsA backbone emerge from the data with characteristic relaxation behavior. These regions are discussed below, in order from the cellular side towards the periplasm (Table 1).

The two intracellular regions at the KcsA termini (residues 16–23 and 120–160) are characterized by elevated $J(\omega_{\text{N}})$ and $J(0.87\omega_{\text{H}})$ values and depressed $J(0)$ values when compared to the KcsATM domain. These results, together with

generalized order parameter (S^2) values of 0.2–0.45 and internal motions on the 1–1.5 ns timescale, imply that the intracellular domains exhibit considerable flexibility. Only the five C-terminal residues exhibit a relaxation pattern characteristic of a fully disordered segment.

A different relaxation pattern is found for residues at the intracellular membrane interface, representing points of entry of the KcsA backbone into the micelle. Residues 24–35 (entering the micelle) exhibit a gradual transitional trend, while a sharper transition is seen for residues 108–119 (exiting the micelle); in both cases backbone rigidity increases as the KcsATM domain is approached. An increase in helical character for

Table 1. Relaxation parameters for KcsA at $\gamma_N B_0 = 60.8$ MHz, $T = 323$ K^a

KcsA domain	Residues	R_1 (s ⁻¹)	R_2 (s ⁻¹) ^b	hetNOE	η_{xy} (s ⁻¹)	S^2	
Cytoplasmic ^c	Overall	16–23	1.21 ± 0.11	20.3 ± 5.4	0.33 ± 0.13	15.0 ± 4.3	0.35 ± 0.10
		120–160					
Helices	16–19	1.17 ± 0.07	22.9 ± 2.5	0.43 ± 0.07	16.8 ± 2.5	0.41 ± 0.04	
	142–155						
Unstructured	20–23	1.22 ± 0.12	18.6 ± 6.1	0.28 ± 0.12	13.9 ± 4.8	0.32 ± 0.11	
	120–141						
	156–160						
Micelle interface ^c	24–35	0.65 ± 0.20	42.0 ± 12.8	0.52 ± 0.21	29.6 ± 11.7	0.75 ± 0.18	
	108–119						
Trans-membrane ^d	36–50	0.30 ± 0.03	60.3 ± 7.5	0.80 ± 0.04	48.7 ± 4.3	0.92 ± 0.07	
	65–79						
	88–107						
Periplasmic ^c	51–64	0.53 ± 0.17	59.8 ± 4.7	0.57 ± 0.16	43.9 ± 10.2	0.93 ± 0.06	
	80–87						

^aData represent average and standard deviation values for the amide sites in the described KcsA domain. ^b R_2 values measured as corrected $R_{1\rho}$ rates (see text). ^cData acquired for KcsA^E in 7% D₂O. ^dData acquired for KcsATM in 99% D₂O.

residues 27–31 evidenced by previous findings (Chill et al., 2006) may account for the disparity between the two interfaces.

The KcsATM domain itself exhibits relatively uniform relaxation parameters, and its relaxation is dominated by global tumbling, as shown by elevated $J(0)$ and S^2 values in the 0.85–0.9 range, with low $J(\omega_N)$ and $J(0.87\omega_H)$ implying negligible contributions of faster motions.

Finally, residues in the extracellular domain of KcsA, comprising the loops connecting TM1, the pore domain, and TM2 (residues 51–64 and 80–88) have intermediate relaxation parameters, generally bearing a closer resemblance to the rigid KcsATM than to the flexible terminal regions. Several residues in this domain are outliers in the TROSY-¹H-¹⁵N-HSQC fingerprint spectrum of tetrameric KcsA, shifting significantly upon monomerization of KcsA (data not shown), indicative of a well-structured environment in the tetramer. Curiously, all three proline residues, which may have a rigidifying effect upon the backbone, are found in this region. Furthermore, mutation of residue D80 in this region affects the tetrameric stability of KcsA (Choi and Heginbotham, 2004). The relaxation data is therefore consistent with the assumption that the extracellular KcsA domain is involved in inter-subunit contacts that rigidify its structure in comparison to the flexible intracellular segments.

Backbone dynamics in the flexible intracellular terminal regions

By nature, the flexible intracellular segments of KcsA defy study by crystallization, whereas NMR is well suited to probe structure and dynamics in this region. As helical segments have been identified along the C-terminal domain (residues 120–160) in previous studies (Cortes et al., 2001), and a possible biological role in facilitating tetramerization has been assigned to it (Molina et al., 2004), this segment is of particular interest in our study. A combination of backbone chemical shifts, ¹H-¹H NOE patterns, and solvent exchange data has previously established that in SDS micelles, residues 142–155 form a helix which is connected to the TM2 domain by a flexible linker, formed by residues 128–136. In addition, the near-absence of interactions between SDS molecules and this segment have been shown by detergent-excitation NOE experiments (Chill et al., 2006). Overall, our present relaxation data suggest this domain to be quite dynamic, with hetNOE values in the 0.2–0.45 range, yet clearly not disordered or denatured, as a comparison to typical relaxation data observed for denatured proteins (Schwalbe et al., 1997; Schwarzsinger et al., 2002) shows.

Spectral density mapping analysis for this segment reveals a minimum in $J(0)$ and a

corresponding maximum of $J(\omega_N)$ at residues 129–130, and a distinct contribution of high frequency motions $J(0.87\omega_H)$ throughout the flexible linker for residues 132–140. Model-free analysis of this domain distinguishes between the linker ($S^2 \sim 0.25$) and the helical segment ($S^2 \sim 0.4$). Indeed, model-free results imply that S^2 values observed for the linker represent the base level of order in the KcsA backbone, observed in two segments only, the other being residues 20–24. Interestingly, S^2 values in the N-terminal domain are consistent with the presence of a short helical segment at the N-terminus of the construct (residues 16–19) used in this study, suggesting the preceding, truncated residues form a helix as well. Given this relaxation behavior, KcsA appears to behave as a large rigid body, with a far smaller structure tethered to it by a flexible linker. We conclude that under our measurement conditions, the occupancy of a state in which all four C-terminal helices in tetrameric KcsA join to form a bundle of helices is minimal. A possible role of this helical region as a tetramerization domain must therefore be investigated under different conditions, possibly with a detergent milder than SDS.

Backbone dynamics of the selectivity filter

The KcsA selectivity filter is a five-residue segment (residues 75–79) immediately following the pore helix, whose backbone carbonyl atoms form coordination cages that can accommodate incoming K^+ ions – but not the far more ubiquitous Na^+ cations – allowing only the former passage into the channel (Doyle et al., 1998). With backbone atoms directly involved in its biological function, backbone dynamics of the selectivity filter are of particular interest. Crystal structures have suggested that the filter may switch between two conformations as a function of K^+ concentration (Zhou and MacKinnon, 2003; Zhou et al., 2001). ^{15}N - and 1H -linewidths of residue V76 were previously shown to increase due to chemical exchange in the presence of as little as 1 mM K^+ at NMR conditions (Chill et al., 2006). Indeed, this residue is the sole amide site determined by model-free analysis to exhibit a significant exchange contribution to transverse relaxation. It is quite plausible (and consistent with triple-resonance spectra for V76) that a small amount of K^+ is present in NMR samples, since they may contain up to 200 mM of Na^+ as the

detergent counter ion, and that the observed broadening reflects switching between the apo- and K^+ -ligated states. Regardless of the actual K^+ sample concentrations, S^2 values for the selectivity filter are only slightly lower than those of the three KcsA helices, and clearly still indicative of a rather rigid structure, with no observable contribution of fast backbone motions to relaxation. Therefore, our results give no indication of large amplitude reorientation of the filter on the ps–ns timescale, and suggest a well-ordered backbone in the selectivity filter for the closed state of KcsA.

Conclusions

We have shown that ^{15}N relaxation parameters can be measured on a per-residue basis even for a large micelle-solubilized protein with significant spectral overlap using 3D-tHNCO-based experiments optimized for suppression of unwanted water and detergent signals. The tetrameric KcsATM domain tumbles as a rigid body and a rotational correlation time that corresponds to the value expected for a ~ 120 kDa protein-detergent aggregate. Moderate internal flexibility is found for some, but not all of the residues in the short loops connecting the three helices. In contrast, the terminal regions, and in particular the C-terminal helix, which maintains a degree of local structure but is not involved in tetramer formation under the conditions used in this study, show extensive internal dynamics. Although KcsA benefits from the remarkable resistance of its transmembrane core to solvent exchange, the experiments presented here should prove generally useful for the study of membrane and other large proteins. The ability to study the flexible and highly overlapping C-terminal domain is important, since such intracellular domains are commonly found in membrane proteins and often may be involved in their biological function. Considering that NMR is a key technology for studying protein dynamics, methods described here should serve to enhance its capabilities in the study of structure and dynamics of membrane proteins. We also note that the implementation and parameterization of the water-flip-back TROSY scheme used in our relaxation experiments requires only very weak gradient pulses, and is used for virtually all triple resonance experiments carried out on cryogenic probes in our laboratory.

Electronic Supplementary Material to this paper is available in electronic form at <http://www.dx.doi.org/10.1007/s10858-006-9071-4> and includes a table summarizing the acquisition parameters for measurement of KcsA relaxation rates, two tables containing all relaxation rates and calculated model-free parameters, a figure describing the 2D-TROSY-HSQC version of the experiment for measuring cross-correlated relaxation, and a figure demonstrating the measurement of relaxation rates using 3D-tHNCO-based experiments.

Acknowledgements

We thank Frank Delaglio for software support, Dennis Torchia (NIDCR/NIH) and Chris Miller (Brandeis University) for helpful discussions and Annie Aniana for assistance in sample preparation. J. H. C. acknowledges the support of a long-term EMBO fellowship. This work was supported by the Intramural Research Program of the NIDDK, NIH, and by the Intramural AIDS-Targeted Antiviral Program of the Office of the Director, NIH.

References

- Akke, M. (2002) NMR methods for characterizing microsecond to millisecond dynamics in recognition and catalysis. *Curr. Opin. Struct. Biol.*, **12**, 642–647.
- Arora, A. and Tamm, L.K. (2001) Biophysical approaches to membrane protein structure determination. *Curr. Opin. Struct. Biol.*, **11**, 540–547.
- Bruschweiler, R. (2003) New approaches to the dynamic interpretation and prediction of NMR relaxation data from proteins. *Curr. Opin. Struct. Biol.*, **13**, 175–183.
- Buevich, A.V., Shinde, U.P., Inouye, M. and Baum, J. (2001) Backbone dynamics of the natively unfolded pro-peptide of subtilisin by heteronuclear NMR relaxation studies. *J. Biomol. NMR*, **20**, 233–249.
- Caffrey, M., Kaufman, J., Stahl, S.J., Wingfield, P.T., Gronenborn, A.M. and Clore, G.M. (1998) 3D NMR experiments for measuring ^{15}N relaxation data of large proteins: application to the 44 kDa ectodomain of SIV gp41. *J. Magn. Res.*, **135**, 368–372.
- Cantor, C.R. and Schimmel, P.R. (1980). *Biophysical Chemistry*, vol. 2, W.H. Freeman and Company, New York. pp. 562–565.
- Carr, P.A., Fearing, D.A. and Palmer, A.G. (1998) 3D-accordion spectroscopy for measuring ^{15}N and ^{13}CO relaxation rates in poorly resolved NMR spectra. *J. Magn. Res.*, **132**, 25–33.
- Chill, J.H., Louis, J.M., Miller, C. and Bax, A. (2006) NMR study of the tetrameric KcsA potassium channel in detergent micelles. *Prot. Sci.*, **15**, 684–698.
- Choi, H. and Heginbotham, L. (2004) Functional influence of the pore helix glutamate in the KcsA K^+ channel. *Biophys. J.*, **86**, 2137–2144.
- Clore, G.M., Driscoll, P.C., Wingfield, P.T. and Gronenborn, A.M. (1990) Analysis of backbone dynamics of interleukin-1-beta using two-dimensional inverse detected heteronuclear ^{15}N - ^1H NMR spectroscopy. *Biochemistry*, **29**, 7387–7401.
- Cole, R. and Loria, J.P. (2003) FAST-Modelfree: a program for rapid automated analysis of solution NMR spin-relaxation data. *J. Biomol. NMR*, **13**, 289–302.
- Copie, V., Tomita, Y., Akiyama, S.K., Aota, S., Yamada, K.M., Venable, R.M., Pastor, R.W., Krueger, S. and Torchia, D.A. (1998) Solution structure and dynamics of linked cell attachment modules of mouse fibronectin containing the RGD and synergy regions: comparison with the human fibronectin crystal structure. *J. Mol. Biol.*, **277**, 663–682.
- Cornilescu, G. and Bax, A. (2000) Measurement of proton nitrogen and carbonyl chemical shielding anisotropies in a protein dissolved in a dilute liquid crystalline phase. *J. Am. Chem. Soc.*, **122**, 10143–10154.
- Cortes, D.M., Cuello, L.G. and Perozo, E. (2001) Molecular architecture of full-length KcsA: role of cytoplasmic domains in ion permeation and activation gating. *J. Gen. Physiol.*, **117**, 165–180.
- Cuello, L.G., Romero, J.G., Cortes, D.M. and Perozo, E. (1998) pH-dependent gating in the *Streptomyces lividans* K^+ channel. *Biochemistry*, **37**, 3229–3236.
- Delaglio, F., Grzesiek, S., Vuister, G.W., Zhu, G., Pfeifer, J. and Bax, A. (1995) NMRPipe: a multidimensional spectral processing system based on UNIX pipes. *J. Biomol. NMR*, **6**, 277–293.
- Doyle, D.A., Cabral, J.M., Pfuetzner, R.A., Kuo, A., Gulbis, J.M., Cohen, S.L., Chait, B.T. and Mackinnon, R. (1998) The structure of the potassium channel: Molecular basis of K^+ conduction and selectivity. *Science*, **280**, 69–77.
- Eisenmesser, E.Z., Bosco, D.A., Akke, M. and Kern, D. (2002) Enzyme dynamics during catalysis. *Science*, **295**, 1520–1523.
- Farrow, N.A., Muhandiram, R., Singer, A.U., Pascal, S.M., Kay, C.M., Gish, G., Shoelson, S.E., Pawson, T., Forman-Kay, J.D. and Kay, L.E. (1994) Backbone dynamics of a free and phosphopeptide-complexed Src homology 2 domain studied by ^{15}N NMR relaxation. *Biochemistry*, **33**, 5984–6003.
- Farrow, N.A., Zhang, O., Szabo, A., Torchia, D.A. and Kay, L.E. (1995) Spectral density function mapping using ^{15}N relaxation data exclusively. *J. Biomol. NMR*, **6**, 153–162.
- Ghose, R., Eykyn, T.R. and Bodenhausen, G. (1999) Average Liouvillian theory revisited: cross-correlated relaxation between chemical shift anisotropy and dipolar couplings in the rotating frame in nuclear magnetic resonance. *Mol. Phys.*, **96**, 1281–1288.
- Goldman, M. (1984) Interference effects in the relaxation of a pair of unlike spin-1/2 nuclei. *J. Magn. Res.*, **60**, 437–452.
- Grey, M.J., Wang, C. and Palmer, A.G. III (2003) Disulfide bond isomerization in basic pancreatic trypsin inhibitor: multisite chemical exchange quantified by CPMG relaxation dispersion and chemical shift modeling. *J. Am. Chem. Soc.*, **125**, 14324–14335.
- Hardy, R.C. and Cottingham, R.L. (1949) Viscosity of deuterium oxide and water from 5 to 125 °C. *J. Chem. Phys.*, **17**, 509–510.
- Heginbotham, L., LeMasurier, M., Kolmakova-Partensky, L. and Miller, C. (1999) Single *streptomyces lividans* K^+

- channels: functional asymmetries sidedness of proton activation. *J. Gen. Physiol.*, **114**, 551–560.
- Ishima, R. and Torchia, D.A. (2000) Protein dynamics from NMR. *Nat. Struct. Biol.*, **7**, 740–743.
- Jones, J.A., Hodgkinson, R., Barker, A.L. and Hore, P.J. (1996) Optimal sampling strategies for the measurement of spin-spin relaxation times. *J. Magn. Res. Ser. B*, **113**, 25–34.
- Kay, L.E. (1998) Protein dynamics from NMR. *Biochem. Cell Biol.*, **76**, 145–152.
- Kay, L.E., Torchia, D.A. and Bax, A. (1989) Backbone dynamics of proteins as studied by ^{15}N inverse detected heteronuclear NMR spectroscopy – application to staphylococcal nuclease. *Biochemistry*, **28**, 8972–8979.
- Kempf, J.G. and Loria, J.P. (2003) Protein dynamics from solution NMR: theory and applications. *Cell Biochem. Biophys.*, **37**, 187–211.
- Kern, D. and Zuiderweg, E.R. (2003) The role of dynamics in allosteric regulation. *Curr. Opin. Struct. Biol.*, **13**, 748–757.
- Korzhev, D.M., Orekhov, V.Y., Dahlquist, F.W. and Kay, L.E. (2003) Off-resonance $R_{1\rho}$ relaxation outside of the fast exchange limit: an experimental study of a cavity mutant of T4 lysozyme. *J. Biomol. NMR*, **26**, 39–48.
- Kroenke, C.D., Loria, J.P., Lee, L.K., Rance, M. and Palmer, A.G. III (1998) Longitudinal and transverse ^1H – ^{15}N dipolar chemical shift anisotropy relaxation interference: unambiguous determination of rotational diffusion tensors and chemical exchange effects in biological macromolecules. *J. Am. Chem. Soc.*, **120**, 7905–7915.
- Lee, D., Hilty, C., Wider, G. and Wuthrich, K. (2006) Effective rotational correlation times of proteins from NMR relaxation interference. *J. Magn. Res.*, **178**, 72–76.
- Lee, L.K., Rance, M., Chazin, W.J. and Palmer, A.G. III (1997) Rotational diffusion anisotropy of proteins from simultaneous analysis of ^{15}N and $^{13}\text{C}\alpha$ nuclear spin relaxation. *J. Biomol. NMR*, **9**, 287–298.
- Lipari, G. and Szabo, A. (1982) Model-free approach to the interpretation of nuclear magnetic resonance relaxation in macromolecules. 1. Theory and range of validity. 2. Analysis of experimental results. *J. Am. Chem. Soc.*, **104**, 4546–4570.
- Lohr, F., Katsemi, V., Hartleib, J., Gunther, U. and Ruterjanz, H. (2003) A strategy to obtain backbone resonance assignments of deuterated proteins in the presence of incomplete amide $^2\text{H}/^1\text{H}$ back-exchange. *J. Biomol. NMR*, **25**, 291–311.
- Loria, J.P., Rance, M. and Palmer, A.G. III (1999) Transverse-relaxation-optimized (TROSY) gradient-enhanced triple-resonance NMR spectroscopy. *J. Magn. Res.*, **141**, 180–184.
- Mandel, A.M., Akke, M. and Palmer, A.G. III (1995) Backbone dynamics of Escherichia coli ribonuclease HI: correlations with structure and function in an active enzyme. *J. Mol. Biol.*, **246**, 144–163.
- McCallum, S.A., Hitchens, T.K. and Rule, G.S. (1999) Solution structure of the carboxyl terminus of a human class μ -glutathione S-transferase: NMR assignment strategies in large proteins. *J. Mol. Biol.*, **285**, 2119–2132.
- Molina, M.L., Encinar, J.A., Barrera, F.N., Fernandez-Ballester, G., Riquelme, G. and Gonzalez-Ros, J.M. (2004) Influence of C-terminal protein domains and protein-lipid interactions on tetramerization and stability of the potassium channel KcsA. *Biochemistry*, **43**, 14924–14931.
- Mulder, F.A., de Graaf, R.A., Kaptein, R. and Boelens, R. (1998) An off-resonance rotating-frame experiment for the investigation of macromolecular dynamics using adiabatic rotations. *J. Magn. Res.*, **131**, 351–357.
- Mulder, F.A., Mittermaier, A., Hon, B., Dahlquist, F.W. and Kay, L.E. (2001) Studying excited states of proteins by NMR spectroscopy. *Nat. Struct. Biol.*, **8**, 932–935.
- Palmer, A.G. III, Kroenke, C.D. and Loria, J.P. (2001) Nuclear magnetic resonance methods for quantifying microsecond-to-millisecond motions in biological macromolecules. *Meth. Enzymol.*, **339**, 204–238.
- Palmer, A.G. III (2001) NMR probes of molecular dynamics: overview and comparison with other techniques. *Annu. Rev. Biophys. Biomol. Struct.*, **30**, 129–155.
- Peng, J.W. and Wagner, G. (1992) Mapping of the spectral densities of N–H bond motions in eglin-C using heteronuclear relaxation measurements. *Biochemistry*, **31**, 8571–8586.
- Pervushin, K., Wider, G. and Wuthrich, K. (1998) Single transition-to-single transition polarization transfer (ST2-PT) in ^{15}N -TROSY. *J. Biomol. NMR*, **12**, 345–348.
- Renner, C., Moroder, L. and Holak, T.A. (2001) Analytical solution to the Lipari-Szabo model based on the reduced spectral density approximation offers a novel protocol for extracting motional parameters. *J. Magn. Res.*, **151**, 32–39.
- Schurr, J.M., Babcock, H.P. and Fujimoto, B.S. (1994) A test of the model-free formulas – effects of anisotropic rotational diffusion and dimerization. *J. Magn. Res. Ser. B*, **105**, 211–224.
- Schwalbe, H., Fiebig, K.M., Buck, M., Jones, J.A., Grimshaw, S.B., Spencer, A., Glaser, S.J., Smith, L.J. and Dobson, C.M. (1997) Structural and dynamical properties of a denatured protein. Heteronuclear 3D NMR experiments and theoretical simulations of lysozyme in 8 M urea. *Biochemistry*, **36**, 8977–8991.
- Schwarzinger, S., Wright, P.E. and Dyson, H.J. (2002) Molecular hinges in protein folding: the urea-denatured state of apomyoglobin. *Biochemistry*, **41**, 12681–12686.
- Silver, M.S., Joseph, R.I., Chen, C.N., Sank, V.J. and Houtt, D.I. (1984) Selective population inversion in NMR. *Nature*, **310**, 681–683.
- Tian, C., Karra, M.D., Ellis, C.D., Jacob, J., Oxenoid, K., Sonnichsen, F. and Sanders, C.R. (2005) Membrane protein preparation for TROSY NMR screening. *Meth. Enzymol.*, **394**, 321–334.
- Tjandra, N., Szabo, A. and Bax, A. (1996) Protein backbone dynamics and ^{15}N chemical shift anisotropy from quantitative measurement of relaxation interference effects. *J. Am. Chem. Soc.*, **118**, 6986–6991.
- Tugarinov, V., Ollerenshaw, J.E. and Kay, L.E. (2005) Probing side-chain dynamics in high molecular weight proteins by deuterium NMR spin relaxation: an application to an 82-kDa enzyme. *J. Am. Chem. Soc.*, **127**, 8214–8225.
- Viles, J.H., Duggan, B.M., Zaborowski, E., Schwarzinger, S., Huntley, J.J.A., Kroon, G.J.A., Dyson, H.J. and Wright, P.E. (2001) Potential bias in NMR relaxation data introduced by peak intensity analysis and curve fitting methods. *J. Biomol. NMR*, **21**, 1–9.
- Wagner, G. and Nirmala, N.R. (1989) Studies of protein dynamics by heteronuclear NMR – individual ^{13}C relaxation times and evidence for multiple conformations in the reactive site of BPTI. *Chem. Scripta*, **29A**, 27–30.
- Wand, A.J. (2001) Dynamic activation of protein function: a view emerging from NMR spectroscopy. *Nat. Struct. Biol.*, **8**, 926–931.

- Weigelt, J. (1998) Single scan sensitivity- and gradient-enhanced TROSY for multidimensional NMR experiments. *J. Am. Chem. Soc.*, **120**, 10778–10779.
- Woessner, D.E. (1962) Nuclear spin relaxation in ellipsoids undergoing rotational Brownian motion. *J. Chem. Phys.*, **37**, 647–654.
- Yu, L.P., Sun, C.H., Song, D.Y., Shen, J.W., Xu, N., Gunasekera, A., Hajduk, P.J. and Olejniczak, E.T. (2005) Nuclear magnetic resonance studies of a potassium channel-charybdotoxin complex. *Biochemistry*, **44**, 15834–15841.
- Zhou, Y. and MacKinnon, R. (2003) The occupancy of ions in the K⁺ selectivity filter: charge balance and coupling of ion binding to a protein conformational change underlie high conduction rates. *J. Mol. Biol.*, **333**, 965–975.
- Zhou, Y., Morais-Cabral, J.H., Kaufman, A. and MacKinnon, R. (2001) Chemistry on ion coordination and hydration revealed by a K⁺ channel-Fab complex at 2.0 Å resolution. *Nature*, **414**, 43–48.
- Zhu, G., Xia, Y., Nicholson, L.K. and Sze, K.H. (2000) Protein dynamics measurements by TROSY-based NMR experiments. *J. Magn. Res.*, **143**, 423–426.